Chemical Engineering Journal 171 (2011) 951–957

Contents lists available at ScienceDirect

Chemical Engineering Journal

journal homepage: www.elsevier.com/locate/cej

Equilibria and kinetics of phenol adsorption on a toluene-modified hyper-cross-linked poly(styrene-co-divinylbenzene) resin

Jianhan Huang[a,b,*], Ruijie Deng[a,b], Kelong Huang[a,b]

[a] School of Chemistry and Chemical Engineering, Central South University, Changsha 410083, China
[b] Key Laboratory of Resources Chemistry of Nonferrous Metals, Ministry of Education (Central South University), Changsha 410083, China

ARTICLE INFO

Article history:
Received 14 March 2011
Received in revised form 14 April 2011
Accepted 20 April 2011

Keywords:
Hyper-cross-linked
Poly(styrene-co-divinylbenzene) resin
Adsorption
Absorption
Isothermal
Kinetics

ABSTRACT

A series of novel toluene-modified hyper-cross-linked poly(styrene-co-divinylbenzene) resins were synthesized and the adsorption behaviors of the synthesized resins toward phenol were investigated from aqueous solution. Among the synthesized five resins, HJ-L15 possessed the largest adsorption capacity toward phenol. The phenol adsorption onto HJ-L15 is combination of the surface adsorption and the absorption due to skeleton swelling. The molecular form of phenol was favorable for the adsorption. The isotherms could be fitted by Freundlich model and the adsorption was shown to be an exothermic process. The kinetic curves could be characterized by pseudo-second-order rate equation and the intra-particle diffusion was the rate-limiting step at the initial stage.

1. Introduction

Macroporous cross-linked poly(styrene-co-divinylbenzene) (PS) or polymethacrylate resins have displayed excellent adsorption behaviors toward aromatic compounds [1–4], and hence these resins are increasingly applied for the efficient removal and recycling of aromatic compounds [5]. In the 1970s, Davankov developed a hyper-cross-linking technique, and a type of novel hyper-cross-linked PS resin was prepared from linear PS or low cross-linked PS through the use of bifunctional cross-linking agents and Friedel–Crafts catalysts [6,7]. The specific surface area of the prepared resin was shown to be relatively high with the pore diameter distribution being dominated by mesopores [8]. Adsorption experiments indicated that the prepared resin displayed excellent adsorption behaviors toward nonpolar or weakly polar aromatic compounds [9–11], whereas its adsorption capacity toward polar aromatic compounds was relatively small.

In order to improve the adsorption capacity of the hyper-cross-linked resin toward polar aromatic compounds, various techniques such as the introduction of polar units into the copolymers, the employment of polar compounds as the cross-linking reagent and the introduction of polar aromatic compounds have been examined [12,13]. The results indicated that the introduction of the polar groups into such resins increased their retention toward polar aromatic compounds [14,15]. In addition, study of the adsorption mechanism revealed that the improved polarity of the hyper-cross-linked resin plays an important role in the enhanced adsorption of the hyper-cross-linked resin toward polar aromatic compounds [16,17].

If low cross-linked chloromethylated PS is applied as the reactant, some non-polar aromatic compound like toluene is also added in the Friedel–Crafts reaction, the Friedel–Crafts reaction between the chloromethylated PS and toluene will also occur in addition to the Friedel–Crafts reaction of the chloromethylated PS itself. Will the adsorption of the obtained toluene-modified hyper-cross-linked resin toward polar aromatic compounds like phenol be enhanced? In addition, because of the addition of a different quantity of toluene in the reaction, the pore structure and the chemical structure of the prepared hyper-cross-linked resin will be different and which will determine the adsorption selectivity of the synthesized resin. To the best of our knowledge, there is few report focusing on synthesis and adsorption behaviors of toluene-modified hyper-cross-linked PS resin so far [18].

In this study, a series of novel hyper-cross-linked PS resins are prepared from macroporous cross-linked chloromethylated PS by adding a different quantity of toluene in the Friedel–Crafts reaction, the pore structures, chemical structures and adsorption capacities of the prepared resins toward phenol are compared. After investigating the adsorption mechanism for the phenol adsorption onto the hyper-cross-linked PS resins, HJ-L15 is selected as the polymeric adsorbent, phenol is chosen as the adsorbate, and the adsorption behaviors of HJ-L15 toward phenol are investigated

* Corresponding author. Tel.: +86 831 8879850; fax: +86 731 88879616.
E-mail address: xiaomeijiangou@yahoo.com.cn (J. Huang).

1385-8947/$ – see front matter © 2011 Elsevier B.V. All rights reserved.
doi:10.1016/j.cej.2011.04.045

from aqueous solution, the equilibria and kinetics of HJ-L15 toward phenol are considered in detail.

2. Experimental method

2.1. Materials

Phenol (Molecular formula: C_6H_6OH, Molecular weight: 94.1) applied as the adsorbate in this study was an analytical reagent and distilled before use. Macroporous cross-linked chloromethylated PS was purchased from Langfang Chemical Co. Ltd. (Hebei, China), the chloromethylated PS had a degree of cross-linking degree of 6%, a chlorine content of 17.3%, a specific surface area of 18.03 m^2/g, a pore volume of 0.0313 cm^3/g and an average pore diameter of 25.7 nm. The Amberlite XAD-4 was kindly provided by Rohm & Haas Company (Philadelphia, USA) and X-5 was bought from the Chemical Plant of Nankai University (Tianjin, China).

2.2. Synthesis of the hyper-cross-linked resins

40 g of the chloromethylated PS was swollen by 120 mL of nitrobenzene and a small quantity of toluene (0%, 5%, 10%, 15% and 20% relative to chloromethylated PS, w/w) over a period of 8 h at room temperature. At a moderate stirring speed, 3.0 g of anhydrous zinc chloride was then added into the reaction mixture at 323 K. About half an hour later, the reaction mixture was heated to 388 K within 1 h. After the reaction mixture was held at 388 K for 10 h, the hyper-cross-linked resins, namely HJ-L00, HJ-L05, HJ-L10, HJ-L15 and HJ-L20 were obtained. The possible Friedel–Crafts reaction taken place and the possible products for the hyper-cross-linked resins were shown in Scheme s1. The hyper-cross-linked resins were filtrated from the reaction mixture and rinsed by 1% of hydrochloric acid and anhydrous ethanol until the effluents from hydrochloric acid were transparent. Subsequently the resins were washed by deionized water until neutral pH, extracted by anhydrous ethanol for 10 h, and dried in vacuum at 323 K for 8 h.

2.3. Characterization of the hyper-cross-linked resins

The specific surface area and pore volume of the resin were determined by N_2 adsorption–desorption isotherms at 77 K using a Micromeritics Tristar 3000 surface area and porosity analyzer (Micromeritics, USA). The total specific surface area and pore volume of the resin were calculated according to Brunauer–Emmett–Teller (BET) model while the micropore specific surface area of the resins was calculated from the pore diameter distribution data, which was calculated by applying the Barrett, Joyner and Halenda (BJH) method, and the pore diameter distribution of the resin was calculated by applying BJH method to the N_2 desorption data. The Fourier transform infrared (FTIR) spectroscopy of the resin with vibrational frequencies in the range of 500–4000 cm^{-1} was collected by KBr disks on a Nicolet 510P FTIR instrument (Nicolet Company, USA). The swelling capacity of the resin was measured as follows. The resin at the dry state and at the swollen state after being swollen in a certain solvent (water, 1% of phenol solution, 10% of phenol solution or liquid phenol) for 24 h was taken photos with the same magnifications, the diameter of the resin was measured and the swelling capacity of the resin (R_v) was calculated as:

$$R_v = \left(\frac{D_t}{D_0}\right)^3 \quad (1)$$

here D_0 and D_t are the diameter of the resin at the dry state and at the swollen state after being swollen in a certain solvent for 24 h, respectively.

2.4. Adsorption

Prior to use, the resin was wetted by 0.5 mL of ethanol and then rinsed three times by deionized water. In an isotherm experiment, about 0.1000 g of the dry resin was accurately weighed and mixed with 50 mL of phenol solution. The initial concentration of phenol solution was set to be about 100–600 mg/L with 100 mg/L interval. Hydrochloric acid and sodium hydroxide were applied to adjust the solution pH. The flasks were then shaken in a thermostatic oscillator for ca. 8 h at a desired temperature (288, 298, 308 or 318 K). A preliminary experiment had proved that the adsorption can reach equilibrium within 8 h. After filtration of the resin from the mixture, the solution was analyzed by UV spectrometry on a UV2450 spectrophotometer (Shimadzu Scientific Instrument Inc., Japan) at a wavelength of 269.9 nm. The concentration of the residual solution was measured and the equilibrium adsorption capacity was calculated as [19]:

$$q_e = \frac{(C_0 - C_e)V}{W} \quad (2)$$

where q_e is equilibrium adsorption capacity (mg/g), C_0 and C_e are the initial and the equilibrium concentration of phenol (mg/L), V is the volume of the solution (L) and W is the weight of the resin (g).

In a kinetic experiment, about 1.0000 g of the resin and 500 mL of phenol solution were quickly introduced into a cone-shaped flask. The initial concentrations of the phenol solution were set to be 415.2, 502.1 or 603.0 mg/L, respectively. The mixture was continuously shaken at 298 K and 0.5 mL of the solution was sampled at different time intervals. The concentration of the residual solution was determined until the adsorption equilibrium was reached and the adsorption capacity at contact time t was calculated as [20]:

$$q_t = \frac{(C_0 - C_t)V}{W} \quad (3)$$

here q_t is the adsorption capacity at contact time t (mg/g) and C_t is the concentration of phenol at contact time t (mg/L).

3. Results and discussion

3.1. Characterization of the hyper-cross-linked resins

Fig. 1(a) displays the specific surface area and pore volume of HJ-L00, HJ-L05, HJ-L10, HJ-L15 and HJ-L20, respectively. It is observed that the specific surface area of the five resins has the same trend as the pore volume. The specific surface area of HJ-L00 is the highest among the five resins (the micropore specific surface areas of the five resins calculated by applying the BJH method are determined to be 229.7, 193.2, 202.9, 163.0 and 112.4 m^2/g, respectively) and it decreases rapidly as adding toluene in the Friedel–Crafts reaction. The reason can be followed that the loaded toluene increases the length of the cross-linking bridge or the neighboring two cross-linking chains [18], and which enlarges the average pore diameter of the resin, decreasing the specific surface area.

Fig. 1(b) indicates that all of the N_2 adsorption isotherms seem close to type-II classification. At the initial part of the adsorption isotherm with a relative pressure below 0.05, the N_2 adsorption capacity increases sharply with increasing the relative pressure, proving that micropores are existent. The visible hysteresis loops of the desorption isotherm indicate that mesopores are also present. These analyses agree with the pore diameter distribution in Fig. 1(c). It can be seen that the Friedel–Crafts reaction results in a great transfer for the pore diameter distribution of the resin, mesopores and macropores are the main pores for the chloromethylated PS and the average pore diameter is 25.7 nm, while mesopores in the range of 2–5 nm play a predominant role for the toluene-modified hyper-cross-linked resins and the aver-

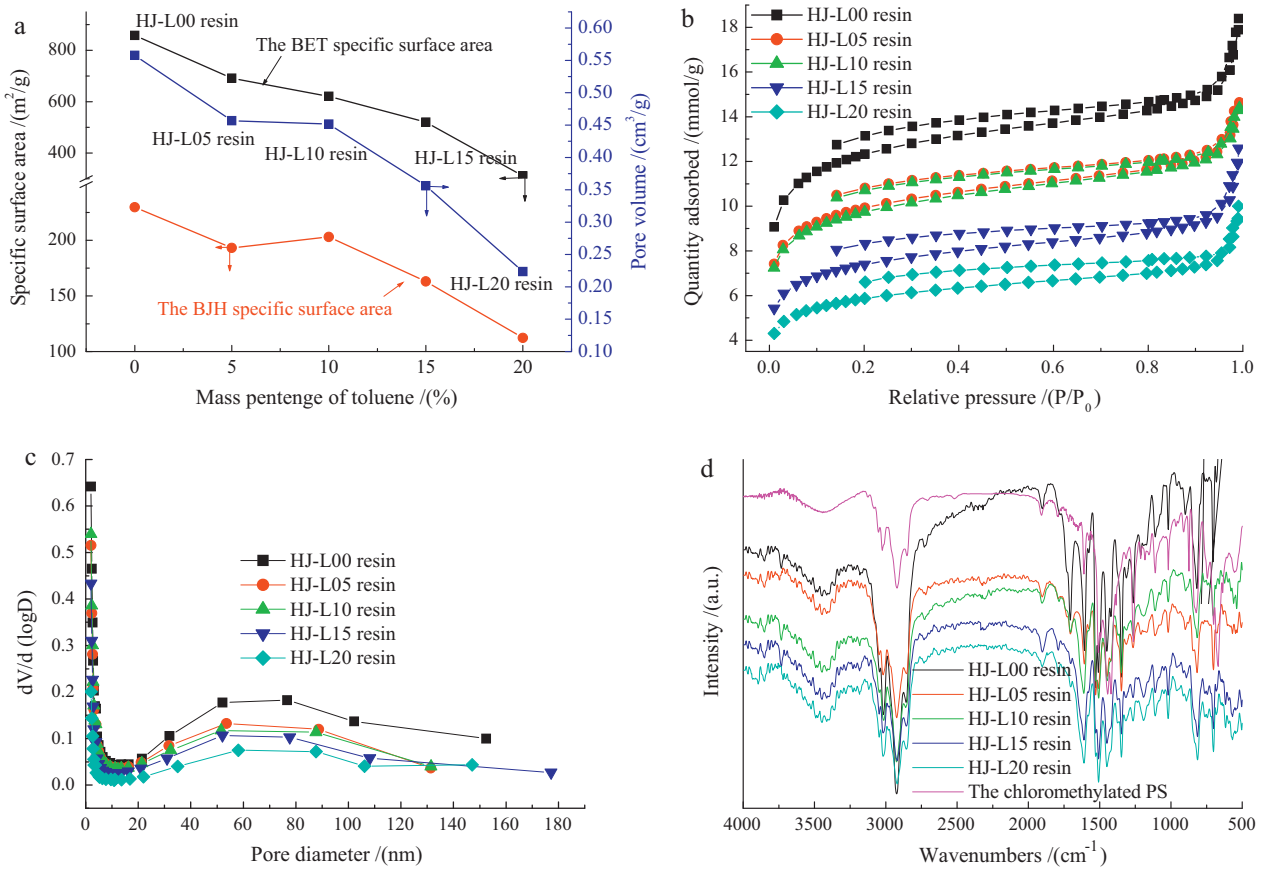

Fig. 1. Characterization of HJ-L00, HJ-L05, HJ-L10, HJ-L15 and HJ-L20 (a) Specific surface area and pore volume; (b) N_2 adsorption–desorption isotherms; (c) pore diameter distribution; (d) FTIR spectra.

age pore diameters of the five resins are 2.41, 2.59, 2.64, 2.65 and 2.73 nm, respectively.

As can be seen from the FTIR spectra of resins in Fig. 1(d), most of the vibrations of the related resins are similar. In addition, two representative vibrations with frequencies at 1265 and 669 cm^{-1} are very strong for the chloromethylated PS, these two vibrations may be assigned to the C–Cl stretching of the CH_2Cl groups [21]. After the Friedel–Crafts reaction, these two vibrations are greatly weakened, while a moderate vibration appears at 1704 cm^{-1} for the toluene-modified hyper-cross-linked resins, this vibration may be assigned to the C=O stretching of formaldehyde due to the oxidation of CH_2Cl groups [21]. In particular, the intensity of the C=O stretching becomes weakened with increasing the quantity of toluene, which may be from the fact that toluene can be oxidized more easily than the chloromethylated PS. Additionally, the characteristic C=C stretching of the benzene ring with frequencies at 1601, 1500 and 1444 cm^{-1} is strengthened after the Friedel–Crafts reaction [21]. These results may demonstrate that toluene be loaded successfully on the surface of the hyper-cross-linked resins.

3.2. Adsorption selectivity

Adsorption isotherms of phenol onto HJ-L00, HJ-L05, HJ-L10, HJ-L15 and HJ-L20 are firstly compared and the results are displayed in Fig. 2. It is interesting to find that HJ-L00 does not possess the largest adsorption capacity toward phenol despite of its highest specific surface area (especially the micropore specific surface area) and pore volume. Additionally, the adsorption capacity of phenol onto the five reins at the same equilibrium concentration follows an order as: HJ-L15 > HJ-L10 > HJ-L05 > HJ-L00 > HJ-L20. That is, with increasing the added quantity of toluene in the Friedel–Crafts reaction, the specific surface area and pore volume of the obtained resin are greatly decreased, while the adsorption of phenol onto the resin is firstly enhanced and then weakened, and HJ-L15 possesses the largest adsorption capacity toward phenol.

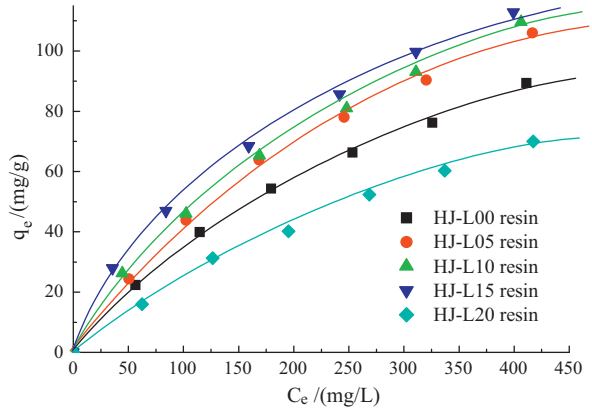

Fig. 2. Comparison of adsorption isotherms of phenol onto HJ-L00, HJ-L05, HJ-L10, HJ-L15 and HJ-L20 from aqueous solution at 298 K.

Langmuir and Freundlich isotherms are two typical models to describe the adsorption process. Langmuir model can be followed as [22]:

$$\frac{C_e}{q_e} = \frac{C_e}{q_m} + \frac{1}{q_m K_L} \quad (4)$$

here q_m is the maximum adsorption capacity (mg/g) and K_L is a characteristic constant (L/mg).

Table 1
The swelling capacity of HJ-L15 in different solvents.

Solvents	Water	1% of phenol solution	10% of phenol solution	Liquid phenol
Swelling capacity	1.22	1.33	1.56	2.35

The Freundlich model can be given as [23]:

$$\log\ q_e = \frac{1}{n} - \log C_e + \log K_F \quad (5)$$

where K_F [(mg/g)(L/mg)$^{1/n}$] and n (dimensionless) are also the characteristic constants. K_F indicates an adsorption interaction between the adsorbent and the adsorbate whereas n is an indicator of the favorableness of the adsorption system.

The corresponding parameters K_L, K_F, n and the correlation coefficients R^2 are summarized in Table S1. It is clear that both of the Langmuir and Freundlich models can characterize the adsorption data of HJ-00 and HJ-L05 since $R^2 > 0.99$, while the Freundlich model is more suitable for the adsorption of HJ-L10, HJ-L15 and HJ-L20. As compared the K_F of the five resins, it firstly increases and then decreases with increasing the added quantity of toluene, accordant with the adsorption capacity of phenol onto the five resins.

3.3. The swelling capacity of the resin and the adsorption mechanism

HJ-L00 has the highest specific surface area and pore volume with some polar formaldehyde carbonyl groups on its surface, while its adsorption capacity toward phenol is a little smaller than HJ-L05, HJ-L10 and HJ-L15, implying that there should some other factors influencing the adsorption except for the specific surface area and polarity of adsorbent [24,25]. Thus, the swelling capacity of HJ-L15 in different solvents is measured and the results are displayed in Table 1 (the photos taken are shown in Fig. s1). It is interesting to see that HJ-L15 can be swollen in the four solvents and the swelling capacity of HJ-L15 in liquid phenol is the highest. As performing the experiment for the adsorption of HJ-L15 toward phenol from aqueous solution, in addition to the surface adsorption of HJ-L15 toward phenol, the skeleton of HJ-L15 can even be swollen by phenol molecules and which increases the adsorption capacity of HJ-L15 toward phenol. In conclusion, the adsorption mechanism can be deduced that the surface adsorption and the absorption due to skeleton swelling play dominant roles in the adsorption of HJ-L15 toward phenol from aqueous solution.

There is a part of mysterious skeleton which is very compact for the hyper-cross-linked resin [26,27], and this very compact skeleton cannot be swollen by solvents and hence is useless for the adsorption. As adding toluene in the Friedel–Crafts reaction, the Friedel–Crafts reaction between toluene and the chloromethylated PS will reduce the percentage of the very compact skeleton of the obtained hyper-cross-linked resin [20]. It can be concluded that the percentage of the very compact skeleton of HJ-L05, HJ-L10 and HJ-L15 should be relatively less than HJ-L00. The improved compact skeleton of the obtained resin by toluene can be swollen by phenol and is usable for the adsorption. As a result, the adsorption capacity of phenol onto HJ-L05, HJ-L10 and HJ-L15 is a little larger than HJ-L00.

3.4. Comparison of adsorption of phenol onto different resins from aqueous solution

The commercial XAD-4 and X-5 are both polystyrene resins with high hydrophobicity [28], and they are considered to be the most efficient polymeric adsorbents for removing aromatic pollutants from wastewater, especially for nonpolar or weakly polar aromatic pollutants such as β-naphthol and phenol [29]. Thus the adsorption isotherm of phenol onto HJ-L15 is thereafter compared with the XAD-4 and X-5. Fig. 3 indicates that HJ-L15 possesses a much larger adsorption capacity toward phenol than XAD-4 and X-5. The specific surface area of HJ-L15 (858.4 m^2/g) is a little lower than XAD-4 (873.1 m^2/g) and higher than X-5 (551.2 m^2/g), the larger adsorption capacity of HJ-L15 toward phenol than XAD-4 may be from the excellent pore structure while the much enhanced adsorption of HJ-L15 in comparison with X-5 may be resulted from the combinations of the specific surface area and the pore structure.

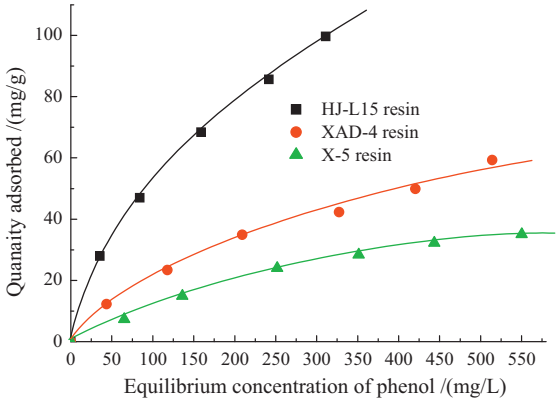

Fig. 3. Comparison of phenol adsorption onto HJ-L15, XAD-4 and X-5 from aqueous solution with the temperature at 298 K.

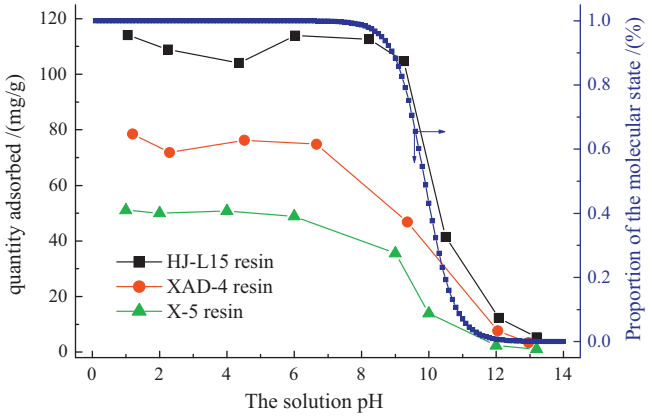

Fig. 4. Effect of the solution pH on the phenol adsorption onto HJ-L15, XAD-4 and X-5 at 298 K.

Langmuir and Freundlich models are adopted to describe the adsorption data, and the corresponding parameters K_L, K_F, n and R^2 are listed in Table s2. It is observed that Freundlich models can characterize the adsorption onto HJ-L15, XAD-4 and X-5, implying that the adsorption of phenol onto the three resins should be a multilayer process and the resins hold surface energetic heterogeneity [3,30]. As compared the K_F and n of the three resins, $K_{F(HJ\text{-}L15)} > K_{F(XAD\text{-}4)} > K_{F(X\text{-}5)}$ and $n_{(HJ\text{-}L15)} > n_{(XAD\text{-}4)} > n_{(X\text{-}5)}$, revealing that the interaction between HJ-L15 and phenol is the greatest and the adsorption of phenol onto HJ-L15 is the most favorable.

3.5. Effect of the solution pH on the adsorption

The effect of the solution pH on the adsorption of phenol onto HJ-L15, XAD-4 and X-5 is illustrated in Fig. 4. pK_a of phenol is 9.89 and the solution pH of the phenol solution in this study is measured to be 6.0, hence the dissociation curve of phenol is predicted and also shown in Fig. 4. The adsorption of phenol onto the three resins has the same trend as the dissociation curve of phenol, implying that

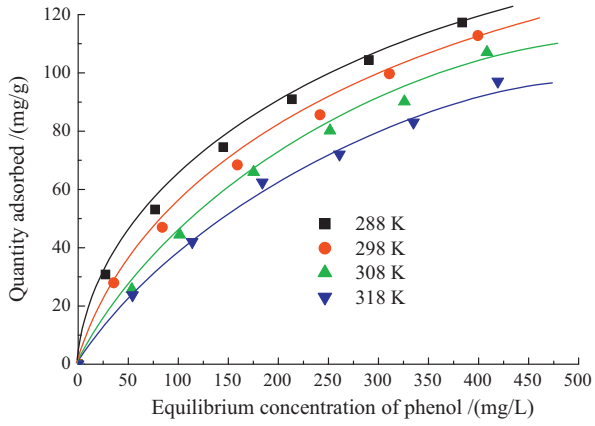

Fig. 5. Adsorption isotherms of phenol onto HJ-L15 from aqueous solution.

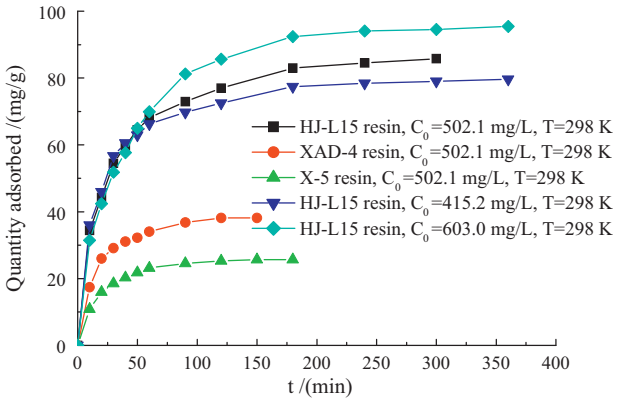

Fig. 6. Adsorption kinetic curves for the phenol adsorption onto HJ-L15, XAD-4 and X-5 from aqueous solution.

the molecular form of phenol is favorable for the adsorption [30]. Phenol is a weak acid and can be ionized in aqueous solution. As the solution pH is higher than 6.0, phenol will be gradually ionized to negative ion, and the adsorption of phenol onto HJ-L15 is weakened. As the solution pH is lower than 6.0, the ionization will be limited, more phenol molecules are attained, and the adsorption of phenol onto HJ-L15 is a little strengthened.

3.6. Adsorption isotherms

As can be seen from Fig. 5 that the adsorption capacity of phenol onto HJ-L15 decreases with increasing the temperature, suggesting an exothermic process [31]. Langmuir and Freundlich models are adopted to describe the adsorption data and the corresponding parameters are listed in Table s3. The Freundlich model is more suitable for the adsorption since $R^2 > 0.99$. With increasing the temperature, the K_F decreases, implying a weaker adsorption driving force at a higher temperature.

According to the Clausius–Clapeyron equation [3,32]:

$$\frac{d\ \ln C_e}{dT} = \frac{\Delta H}{RT^2} \tag{6}$$

where ΔH is the adsorption enthalpy (kJ/mo1) and R is the ideal gas constant. Eq. (7) can be followed by an integral method below:

$$\ln\ C_e = -\frac{\Delta H}{RT} + C' \tag{7}$$

where C' is the integral constant. By plotting the isosters as $\ln C_e$ against $1/T$ (Fig. s2), it is found that the isosters can be fitted to straight lines, and ΔH can be calculated from the slopes of the straight lines.

The Gibbs equation is usually written as [33]:

$$\Gamma = -\frac{c}{RT}\frac{d\gamma}{dc} \tag{8}$$

where c is the concentration, γ is the decrease in the surface free energy and Γ is the surface excess. Eq. (8) can be re-written as:

$$d\gamma = \frac{-\Gamma RT}{c}\ dc \tag{9}$$

Integrating Eq. (9) will give:

$$\Pi = \int d\gamma = -RT\int_0^C \frac{\Gamma\ dc}{c} \tag{10}$$

For the adsorption from the solution, Π represents the change in the surface free energy, i.e. the surface pressure of the solvent–solid interface caused by the adsorption of the solute. Hence the standard adsorption free energy can be followed as:

$$\Delta G = \frac{\Pi}{\Gamma} = -\frac{RT}{\Gamma}\int_0^C \frac{\Gamma\ dc}{c} \tag{11}$$

here ΔG is the standard adsorption free energy (kJ/mol). As the adsorption can be fitted by the Freundlich model and the Gibbs equation will be:

$$\Gamma = K_F c^{1/n} \tag{12}$$

Incorporating Eq. (12) into Eq. (11) will yield:

$$\Delta G = -\frac{RT}{K_F c^{1/n}}\int_0^C \frac{K_F c^{1/n}\,dc}{c}$$

$$= -\frac{RT}{c^{1/n}}\int_0^C c^{1-n/n}\,dc = -\frac{RT}{c^{1/n}} nc^{1/n}\Big|_0^C = -nRT \tag{13}$$

here n is the characteristic constant in Freundlich model.

Adsorption entropy ΔS (J/(mol K)) can be calculated by Gibbs–Helmholtz equation:

$$\Delta S = \frac{\Delta H - \Delta G}{T} \tag{14}$$

Table 2 lists the ΔH, ΔG and ΔS of phenol adsorbed onto HJ-L15 from aqueous solution. The ΔH is negative, indicating an exothermic process [31]. The ΔH decreases with increasing the phenol adsorption on HJ-L15, which is resulted from the surface energetic heterogeneity [3]. The ΔG is also negative, which shows the adsorption is a spontaneous process. The ΔS is negative, revealing that a more ordered arrangement of phenol is shaped on the surface of HJ-L15 after the adsorption.

3.7. Adsorption kinetics

Fig. 6 displays the kinetic curves for the phenol adsorption onto HJ-L15, XAD-4 and X-5 from aqueous solution. It is obvious that the phenol adsorption onto XAD-4 and X-5 can reach equilibrium within 200 min while the required time from the beginning to the equilibrium for the adsorption onto HJ-L15 is about 400 min. In addition, the adsorption capacity of phenol onto HJ-L15 is much larger than that onto XAD-4 and X-5, and a lower initial concentration of phenol results in a shorter required time with a smaller adsorption capacity.

Table 2
The thermodynamic parameters for the adsorption of phenol onto HJ-L15 from aqueous solution.

q_e/(mg/g)	$-\Delta H$/(kJ/mol)	-ΔG/(kJ/mol)				$-\Delta S$/(J/(mol K))			
		288 K	298 K	308 K	318 K	288 K	298 K	308 K	318 K
20	35.36	4.681	4.284	3.734	3.876	106.5	104.3	102.7	99.01
30	29.34	4.681	4.284	3.734	3.876	85.62	84.08	83.14	80.08
40	25.60	4.681	4.284	3.734	3.876	72.64	71.53	70.99	68.31
50	23.38	4.681	4.284	3.734	3.876	64.93	64.08	63.79	61.33
60	20.61	4.681	4.284	3.734	3.876	55.31	54.79	54.79	52.62
70	18.71	4.681	4.284	3.734	3.876	48.71	48.41	48.62	46.65
80	15.90	4.681	4.284	3.734	3.876	38.95	38.98	39.5	37.81

The pseudo-first-order and pseudo-second-order kinetic models assume that the adsorption is a pseudo-chemical reaction and the adsorption rate can be determined as [34,35]:

$$\frac{dq_t}{dt} = k_1(q_e - q_t) \tag{15}$$

$$\frac{dq_t}{dt} = k_2(q_e - q_t)^2 \tag{16}$$

here k_1 (min^{-1}) and k_2 (g/(mg·min)) are the pseudo-first-order and pseudo-second-order rate constants, respectively.

Integrating Eqs. (15) and (16) will give:

$$\ln(q_e - q_t) = \ln\ q_e - k_1 t \tag{17}$$

$$\frac{1}{q_t} = \frac{1}{k_2 q_e^2} + \frac{t}{q_e} \tag{18}$$

If the adsorption follows the pseudo-first-order rate equation, a plot of $\ln(q_e - q_t)$ versus t should be a straight line. On the other hands, t/q_t should change linearly with t if the adsorption obeys the pseudo-second-order rate equation. Available studies have shown that the pseudo-second-order rate equation is a reasonably good fit of data over the entire fractional approach to equilibrium and therefore has been employed extensively in this study of adsorption kinetics [36,37]. Plotting of t/q_t versus t for the phenol adsorption onto HJ-L15 is determined and the fitted correlation parameters are summarized in Table s4. It is clear that the pseudo-second-order rate equation characterizes the adsorption well due to $R^2 > 0.99$. In particular, the adsorption of phenol onto XAD-4 and X-5 has a much greater rate constant than HJ-L15, and a lower initial concentration of phenol results in a greater rate constant.

In common, the intra-particle diffusion is the rate-limiting step for the adsorption of aromatic compounds onto hyper-cross-linked resin from aqueous solution [30]. Therefore, the kinetic data are further dealt with by the intra-particle diffusion model as [38,39]:

$$q_t = k_d t^{1/2} + C \tag{19}$$

where k_d is the intra-particle diffusion rate (mg/(g $min^{1/2}$)), and C is a constant.

If plots of q_t versus $t^{1/2}$ give a straight line and the straight line passes through the origin, the intra-particle diffusion is the rate-limiting step for the adsorption. While if it presents a multi-linear relationship or does not pass through the origin, two or more diffusion mechanisms affect the adsorption [40]. Fig. s3 shows that they yield a three-stage process. At the initial stage, it poses a linear relationship and the straight lines pass through the origin, indicating that the intra-particle diffusion is the rate-limiting step. At the second stage, plots of q_t versus $t^{1/2}$ also yield linear relationships but do not pass through the origin, revealing that multi-diffusion mechanisms are involved.

4. Conclusion

We have synthesized a series of toluene-modified hyper-cross-linked PS resins. As the added quantity of toluene in the Friedel–Crafts reaction is set to be 15% relative to the chloromethylated PS, the adsorption capacity of phenol is the largest. The adsorption of phenol onto HJ-L15 from aqueous solution is the surface adsorption together with the absorption due to skeleton swelling and HJ-L15 is superior to the commercial XAD-4 and X-5. The molecular form of phenol is favorable for the adsorption. Freundlich model depicts the adsorption isotherms better than the Langmuir model and adsorption enthalpy, adsorption free energy and adsorption entropy are all negative. The pseudo-second-order rate equation characterizes the kinetic curves well and the intra-particle diffusion is the rate-limiting step at the initial adsorption process.

Acknowledgments

The research was supported by the National Natural Science Foundation of China (No. 20804058), the Third Shenghua Yuying project of Central South University and the undergraduate innovative experiment project (No. LC10211).

Appendix A. Supplementary data

Supplementary data associated with this article can be found, in the online version, at doi:10.1016/j.cej.2011.04.045.

References

[1] J.S. Fritz, J.N. Story, Selectivity behavior of low-capacity, partially sulfonated, macroporous resin beads, J. Chromatogr. 90 (1974) 267–274.
[2] P. Krisanangkura, A.M. Packard, J. Burgher, F.D. Blum, Bound fractions of methacrylate polymers adsorbed on silica using FTIR, J. Polym. Sci. B 48 (2010) 1911–1918.
[3] H.T. Li, M.C. Xu, Z.Q. Shi, B.L. He, Isotherm analysis of phenol adsorption on polymeric adsorbents from nonaqueous solution, J. Colloid Interf. Sci. 271 (2004) 47–54.
[4] I. Nischang, O. Brueggemann, On the separation of small molecules by means of nano-liquid chromatography with methacrylate-based macroporous polymer monoliths, J. Chromatogr. A 1217 (2010) 5389–5397.
[5] I. Nischang, O. Brueggemann, F. Svec, Advances in the preparation of porous polymer monoliths in capillaries and microfluidic chips with focus on morphological aspects, Anal. Bioanal. Chem. 397 (2010) 953–960.
[6] G.I. Rozenberg, A.S. Shabaeva, V.S. Moryakov, T.G. Musin, M.P. Tsyurupa, V.A. Davankov, Sorption properties of hypercrosslinked polystyrene sorbents, React. Polym. 1 (1983) 175–182.
[7] M.P. Tsyurupa, T.A. Mrachkovskaya, L.A. Maslova, G.I. Timofeeva, L.V. Dubrovina, E.F. Titova, V.A. Davankov, V.M. Menshov, Soluble intramolecularly hypercrosslinked polystyrene, React. Polym. 19 (1993) 55–66.
[8] K. Kondo, Y. Ito, Positron annihilation study of hyper-Cross-Linked polystyrene networks, Macromolecules 35 (2002) 9723–9729.
[9] C.H. Hong, W.M. Zhang, B.C. Pan, L. Lv, Y.Z. Han, Q.X. Zhang, Adsorption and desorption hysteresis of 4-nitrophenol on a hyper-cross-linked polymer resin NDA-701, J. Hazard. Mater. 168 (2009) 1217–1222.
[10] B.C. Pan, W. Du, W.M. Zhang, X. Zhang, Q.R. Zhang, B.J. Pan, L. Lv, Q.X. Zhang, J.L. Chen, Improved adsorption of 4-nitrophenol onto a novel hyper-cross-linked polymer, Environ. Sci. Technol. 41 (2007) 5057–5062.
[11] Y.G. Fan, Z.Q. Shi, R.F. Shi, B.L. He, Post-crosslinking reaction of chloromethylated polystyrene with aromatic hydrocarbons, Ion Exch. Ads. 14 (1998) 31–35.
[12] N. Fontanals, P.A.G. Cormack, D.C. Sherrington, Hypercrosslinked polymer microspheres with weak anion-exchange character: Preparation of the microspheres and their applications in pH-tuneable, selective extractions of analytes from complex environmental samples, J. Chromatogr. A 1215 (2008) 21–29.

[13] N. Fontanals, M. Galia, P.A.G. Cormack, R.M. Marce, D.C. Sherrington, F. Borrull, Evaluation of a new hypercrosslinked polymer as a sorbent for solid-phase extraction of polar compounds, J. Chromatogr. A 1075 (2005) 51–56.
[14] B.J. Brune, J.A. Koehler, P.J. Smith, G.F. Payne, Correlation between adsorption and small molecule hydrogen bonding, Langmuir 15 (1999) 3987–3992.
[15] D. Bratkowska, R.M. Marce, P.A.G. Cormack, D.C. Sherrington, F. Borrull, N. Fontanals, Synthesis and application of hypercrosslinked polymers with weak cation-exchange character for the selective extraction of basic pharmaceuticals from complex environmental water samples, J. Chromatogr. A 1217 (2010) 1575–1582.
[16] B.C. Pan, Q.X. Zhang, F.W. Meng, X.T. Li, X. Zhang, J.Z. Zheng, W.M. Zhang, B.J. Pan, J.L. Chen, Sorption enhancement of aromatic sulfonates onto an aminated hyper -cross-linked polymer, Environ. Sci. Technol. 39 (2005) 3308–3313.
[17] X.M. Wang, J.H. Huang, K.L. Huang, Surface chemical modification on hypercross-linked resin by hydrophilic carbonyl and hydroxyl groups to be employed as a polymeric adsorbent for adsorption of p-aminobenzoic acid from aqueous solution, Chem. Eng. J. 162 (2010) 158–162.
[18] M.C. Xu, Z.Q. Shi, B.L. He, Structure and adsorptive properties of the hypercross-linked polystyrene adsorbents, Acta Polym. Sin. 4 (1996) 446–448.
[19] I. Nischang, F. Svec, J.M.J. Frechet, Effect of capillary cross-section geometry and size on the separation of proteins in gradient mode using monolithic poly(butyl methacrylate-co-ethylene dimethacrylate) columns, J. Chromatogr. A 1216 (2009) 2355–2361.
[20] M.Y. Chang, R.S. Juang, Adsorption of tannic acid, humic acid, and dyes from water using the composite of chitosan and activated clay, J. Colloid Interf. Sci. 278 (2004) 18–25.
[21] J.T. Wang, Q.M. Hu, B.S. Zhang, Y.M. Wang, Organic Chemistry, Nankai University Press, Tianjing, 1998.
[22] S. Balci, Nature of ammonium ion adsorption by sepiolite: analysis of equilibrium data with several isotherms, Water Res. 38 (2004) 1129–1138.
[23] O. Gulnaz, A. Kaya, F. Matyar, B. Arikan, Sorption of basic dyes from aqueous solution by activated sludge, J. Hazard. Mater. 108 (2004) 183–188.
[24] C.O. Ania, B. Cabal, J.B. Parra, A. Arenillas, B. Arias, J.J. Pis, Naphthalene adsorption on activated carbons using solvents of different polarity, Adsorption 14 (2008) 343–355.
[25] G.O. Wood, Affinity coefficients of the Polanyi/Dubinin adsorption isotherm equations. A review with compilations and correlations, Carbon 39 (2001) 343–356.
[26] K. Allmer, A. Hult, B. Raanby, Surface modification of polymers. III. Grafting of stabilizers onto polymer films, J. Polym. Sci. A 27 (1989) 3405–3417.
[27] L.M. Landoll, D.S. Breslow, Polypropylene ionomers, J. Polym. Sci. A 27 (1989) 2189–2201.
[28] I.B. Solangi, S. Memon, M.I. Bhanger, Removal of fluoride from aqueous environment by modified Amberlite resin, J. Hazard. Mater. 171 (2009) 815–819.
[29] Y. Ku, K.C. Lee, Removal of phenols from aqueous solution by XAD-4 resin, J. Hazard. Mater. 80 (2000) 59–68.
[30] J.H. Huang, Adsorption properties of a microporous and mesoporous hypercrosslinked polymeric adsorbent functionalized with phenoxy groups for phenol in aqueous solution, J. Colloid Interf. Sci. 339 (2009) 296–302.
[31] B.L. He, W.Q. Huang, Ion Exchange and Adsorption Resin, Shanghai Science and Education Press, Shanghai, 1995.
[32] J.H. Huang, X.G. Wang, K.L. Huang, Adsorption of p-nitroaniline by phenolic hydroxyl groups modified hyper-cross-linked polymeric adsorbent and XAD-4: a comparative study, Chem. Eng. J. 155 (2009) 722–728.
[33] S.G. Daniel, The adsorption on metal surfaces of long chain polar compounds from hydrocarbon solutions, Trans. Farad. 67 (1951) 439–441.
[34] X.Y. Yang, B. Al-Duri, Kinetic modeling of liquid-phase adsorption of reactive dyes on activated carbon, J. Colloid Interf. Sci. 287 (2005) 25–34.
[35] L.J. You, Z.J. Wu, T. Kim, K. Lee, Kinetics and thermodynamics of bromophenol blue adsorption by a mesoporous hybrid gel derived from tetraethoxysilane and bis(trimethoxysilyl)hexan, J. Colloid Interf. Sci. 300 (2006) 526–535.
[36] J.H. Yoon, J.I. Baek, Y. Yamamoto, T. Komai, T. Kawamura, Kinetics of removal of carbon dioxide by aqueous 2-amino-2-methyl-1,3-propanediol, Chem. Eng. Sci. 58 (2003) 5229–5237.
[37] S. Paul, A.K. Ghoshal, B. Mandal, Kinetics of absorption of carbon dioxide into aqueous solution of 2-(1-piperazinyl)-ethylamine, Chem. Eng. Sci. 64 (2009) 313–321.
[38] W.J. Weber, J.C. Morris, J. Sanit, Eng. Div. Am. Soc. Civ. Eng. 89 (1963) 31–35.
[39] J.H. Huang, G. Wang, K.L. Huang, Enhanced adsorption of salicylic acid onto a β-naphthol-modified hyper-cross-linked poly(styrene-co-divinylbenzene) resin from aqueous solution, Chem. Eng. J. 168 (2011) 715–721.
[40] Z.L. Zhu, A.M. Li, L. Yan, F.Q. Liu, Q.X. Zhang, Preparation and characterization of highly mesoporous spherical activated carbons from divinylbenzene-derived polymer by $ZnCl_2$ activation, J. Colloid Interf. Sci. 316 (2007) 628–634.